PROSPECT-D: towards modeling leaf optical properties through a complete lifecycle

J.B. Féret, A.A. Gitelson, S.D. Noble, S. Jacquemoud

HAL Id: hal-01584365
https://hal.science/hal-01584365

1   PROSPECT-D: towards modeling leaf optical properties through a complete lifecycle

2   J.-B. Féret[1], A.A. Gitelson[2,3], S.D. Noble[4], S. Jacquemoud[5]

3   [1]Irtsea, UMR TETIS, Maison de la Télédétection, 500 Rue Jean François Breton, 34000 Montpellier,
4   France

5   [2]Faculty of Civil and Environmental Engineering, Israel Institute of Technology, Technion City, Haifa,
6   Israel

7   [3]School of Natural Resources, University of Nebraska, Lincoln, USA

8   [4]College of Engineering, University of Saskatchewan, 57 Campus Drive, Saskatoon, SK, S7N 5A9,
9   Canada

10   [5]Institut de physique du globe de Paris - Sorbonne Paris Cité, Université Paris Diderot, UMR CNRS
11   7154, Case 7071, 35 rue Hélène Brion, 75013 Paris, France

12   **Date:** Friday, January 13, 2017

15   **Abstract**

16   Leaf pigments provide valuable information about plant physiology. High resolution monitoring of

17   their dynamics will give access to better understanding of processes occurring at different scales, and

18   will be particularly important for ecologists, farmers, and decision makers to assess the influence of

19   climate change on plant functions, and the adaptation of forest, crop, and other plant canopies. In

20   this article, we present a new version of the widely-used PROSPECT model, hereafter named

21   PROSPECT-D for dynamic, which adds anthocyanins to chlorophylls and carotenoids, the two plant

22   pigments in the current version. We describe the evolution and improvements of PROSPECT-D

23   compared to the previous versions, and perform a validation on various experimental datasets. Our

24   results show that PROSPECT-D outperforms all the previous versions. Model prediction uncertainty is

25   decreased and photosynthetic pigments are better retrieved. This is particularly the case for leaf

26   carotenoids, the estimation of which is particularly challenging. PROSPECT-D is also able to simulate

27   realistic leaf optical properties with minimal error in the visible domain, and similar performances to

28   other versions in the near infrared and shortwave infrared domains.

29   **1. Introduction**

30   Climate change is expected to affect vegetation worldwide, influencing air temperature,

31   biogeochemical cycles, and the frequency and intensity of plant disease. Leaf pigments are key

32   components of life on Earth: they are major contributors to individual plant health via complex

33   mechanisms allowing photosynthesis, plant growth, protection, adaptation to environmental

34   changes and phenological events. Their dynamics directly affects nutrient, nitrogen, carbon and

35   water cycles (Shipley et al., 2006; Joiner et al., 2011). Leaf pigments are therefore good indicators of

36   changes in environmental conditions from local to global scales.

37   Three main families of pigments are found in leaves: chlorophylls, carotenoids, and

38   anthocyanins. Chlorophyll–*a* and –*b*, the two types of molecules in higher plants, are the

39   fundamental light-absorbing pigments involved in photosynthesis. Carotenoids are accessory

40   pigments that contribute to light-harvesting and they also have essential photo-protective

41   properties. If xanthophylls and carotenes are the two major divisions of the carotenoid group, more

42   than 700 naturally occurring molecules have been identified so far, mainly in tissues other than

43   leaves (Britton et al., 2004). Anthocyanins are part of the flavonoid family: they are closely associated

44   with the colors in the autumn foliage of deciduous plant species. The term anthocyanin (*anthos* being

45   Greek for flower, and *kyanos* for blue) has been used since Marquart (1835) to represent the coloring

46   matter responsible for the various colors found in flowers, fruits and foliage in many plant species.

47   The exception are the core Caryophyllales, most of which produce betalains (betacyanins and

48   betaxanthins) (Brockington et al., 2011). While these betalain-producing families do include several

49   species of notable agronomic interest, both crops and weeds, they represent a small fraction of

50   plants investigated in a remote sensing context and are not considered in this work.

51   The anthocyanins include over 500 molecules, which accumulate in the vacuoles of various

52   cells and tissues. They create a pink, red, purple or blue coloration in the tissue depending on the

53   molecule, temperature, pH, and the presence or not of other molecules that may interact with them

54   (Davies, 2004; Gould et al., 2009). Their role is still not fully understood and described. For example,

55   until recently their biosynthesis during senescence was suspected to be nature's extravagancy

56   without a vital function, resulting from evolution in the absence of selection (Matile, 2000), and the

57   reason for their presence was explained as a by-product of the flavonoid biosynthetic pathway.

58   However, research over the past twenty years has demonstrated multiple functional implications of

59   these pigments during the plant life cycle, to the point that they have been called the "Nature's Swiss

60   army knife" by Gould (2004). Among the identified functions of anthocyanins are the protection of

61   the photosynthetic apparatus from damage due to excess light (Lee and Gould, 2002), environmental

62   stresses such as freezing or air pollution, plant pathogens, and predation (Lev-Yadun and Gould,

63   2008). An exhaustive review of the role of anthocyanins in plant leaves can be found in (Davies, 2004)

64   and (Gould, 2004).

65   Leaf pigments interact with solar radiation and change in response to environmental

66   conditions to optimize plant metabolism following complex pathways, within constraints of available

67   resources and stressors. As a result, leaf optical properties are directly impacted by the composition

68   of pigments. Remote sensing has proved to be a particularly suitable tool for the estimation of leaf

69   pigments, both at level of the leaf (e.g., Féret et al., 2008; Gitelson et al., 2006; le Maire et al., 2004;

70   Richardson et al., 2002; Sims and Gamon, 2002) and the canopy (e.g., Asner et al., 2015b; Atzberger

71   et al., 2010; Gitelson et al., 2005; Haboudane, 2004; Hmimina et al., 2015). The retrieval of pigment

72   content from remote sensing data involves two main approaches. The first approach is data-driven. It

73   includes univariate statistical models derived from spectral indices (e.g., Gitelson et al., 2006),

74   multivariate statistical models such as partial least squared regressions (e.g., Asner and Martin, 2009)

75   and machine learning algorithms (e.g., Verrelst et al., 2015). The relationships derived from these

76   predictive models are usually established empirically; they strongly depend on the variability and

77   quality of the data used to adjust these models, therefore they may lack robustness. The second

78   approach is based on radiative transfer models that exist both at leaf and canopy scales. Leaf models

79   generally simulate their spectral directional-hemispherical reflectance and transmittance while

80   canopy models simulate their spectral and bidirectional reflectance assuming that the leaf and soil

81   optical properties, the vegetation architecture, and the conditions of acquisition are known. The

82   combination of the two approaches (data-driven and physical) is also becoming increasingly popular

83   because it provides alternatives to extensive data collection required by the first, and high

84   computational resources required by the second (Féret et al., 2011; Verrelst et al., 2015).

85   To date, most studies devoted to vegetation pigments have focused on chlorophyll. This can be

86   explained by multiple factors. First, leaf chlorophyll content is the variable that has the strongest

87   effect on canopy reflectance in the VIS, and is a valuable proxy of nitrogen content and gross primary

88   production (e.g., Gitelson et al., 2012; Peng and Gitelson, 2012), which have strong impact in terms

89   of food and biomass production globally. Second, leaf chlorophyll content can be estimated with

90   relatively good accuracy using simple statistical regression models based on the relationship between

91   this variable and various spectral indices (e.g. Féret et al., 2011; Gitelson et al., 2006; le Maire et al.,

92   2004). Third, the availability of physical models including chlorophyll as input parameters allowed

93   investigating and better understanding its influence on the signal measured by satellite sensors,

94   leading to improved predictive models for leaf and canopy chlorophyll content in a more systematic

95   way than experimental data collection would have permitted. This is the case of the combined

96   PROSPECT leaf optical properties model (Jacquemoud and Baret, 1990) and SAIL canopy bidirectional

97   reflectance model (Verhoef, 1984; Verhoef et al., 2007), also referred to as PROSAIL, which has been

98   used for more than 25 years (Jacquemoud et al., 2009).

99   Current challenges such as food security, global warming and massive biodiversity loss now

100   require fine monitoring of vegetation status, with a level of information beyond inputs provided by

101   chlorophyll content alone. We need to address various issues related to vegetation, including stress,

102   invasive species, plant diseases and photosynthetic phenology, which implies monitoring the

103   dynamic of various pigment types such as carotenoids (Gamon et al., 2016) and anthocyanins. One of

104   the most studied "pigment-related" indicators derived from remote sensing is the Photochemical

105   Reflectance Index (PRI, Gamon et al., 1992) based on two narrow spectral bands in the green

106   spectrum: the PRI related to the xanthophyll cycle in the leaf; it captures the physiological response

107 of vegetation in response to a short term environmental stress inducting slight changes in

108 photosynthetic activity (Gamon et al., 1997, 1992, 1990). However, the primary driver of the PRI over

109 long time periods, at both leaf and canopy scales, is not the xanthophyll cycle, but rather the

110 changing leaf carotenoid pigment pool, typically expressed as the changing ratio of chlorophyll to

111 carotenoid pigments (or its inverse) (Filella et al., 2009; Nakaji et al., 2006; Stylinski et al., 2002).

112 Therefore, information about pigment content in vegetation is crucial when monitoring

113 photosynthetic phenology. At local scale, estimating pigment content from individuals using portable

114 devices, close range remote sensing or UAV can be useful for monitoring purposes in precision

115 agriculture or ecophysiology. At global scale, the ability to precisely monitor photosynthetic

116 phenology with satellite imagery is extremely valuable and would provide important input for models

117 of global terrestrial carbon uptake. Few studies focus on the direct estimation of carotenoids at leaf

118 scale (Chappelle et al., 1992; Gitelson et al., 2006, 2001; Sims and Gamon, 2002) and canopy scale

119 (Asner et al., 2015a, 2015b; Gamon et al., 2016; Hernández-Clemente et al., 2014, 2012; Ustin et al.,

120 2009; Zarco-Tejada et al., 2013). Even fewer focus on the estimation of anthocyanin, also at leaf

121 (Gamon and Surfus, 1999; Gitelson et al., 2001, 2006; Sims and Gamon, 2002; Steele et al., 2009) and

122 canopy (Rundquist et al., 2014) scales. The presence of overlapping features in the specific

123 absorption coefficient (SAC) of carotenoids and anthocyanins makes it difficult to separate and

124 quantify these accessory pigments using basic methods such as spectral indices, especially at canopy

125 scale (Ustin et al., 2009).

126   Monitoring vegetation status, stress, and shifts in the ecosystem functional properties is

127 critical. It will require sophisticated methods of leaf pigment content estimation, possibly combined

128 with the next generation of high resolution imaging spectrometers like Hyspiri (NASA), EnMAP (DLR)

129 or Hypxim (CNES), and vegetation radiative transfer models that incorporate all major pigments.

130 Present leaf optical properties models do not include pigments other than chlorophylls and

131 carotenoids, limiting the application of the physical approach to the study of these pigments

132 (Blackburn, 2007). SLOP (Maier et al., 1999), PROSPECT-5 (Féret et al., 2008), and soon after LIBERTY,

133 specifically designed for pine needles (Di Vittorio, 2009), are the three models that use carotenoids.

134 The dorsiventral leaf model designed by Stuckens et al. (2009) also differentiates chlorophylls from

135 carotenoids, but the SACs are those used in PROSPECT-5.

136   This article introduces a new version of the widely-used PROSPECT model, called PROSPECT-D,

137 which for the first time includes all three main pigments that control the optical properties of fresh

138 leaves, i.e., chlorophylls, carotenoids, and anthocyanins. The suffix -D stands for "dynamic" because

139 the model makes it possible to simulate leaf optical properties through a complete lifecycle, from

140 emergence, to anthocyanin-expressing stress responses, through to senescence. Given the success

141 and widespread use of PROSPECT-5, a major requirement for the development of PROSPECT-D was

142 to preserve, and ideally to improve on, the performance of PROSPECT-5 for pigment estimation in

143 samples containing little or no anthocyanin, while adding support for those that do. We performed a

144 new calibration of the SAC of each pigment, and updated the refractive index used by the model.

145 PROSPECT-D was then tested on several datasets displaying many plant species with a large range of

146 leaf traits including pigment composition. We evaluated its performance using two criteria resulting

147 from iterative optimization of leaf chemical and structural properties: the difference between the

148 measured and the modeled leaf directional-hemispherical reflectance and transmittance spectra,

149 and the accuracy of corresponding pigment estimation. We compared these two criteria for the new

150 and current versions of the model.

151

152 **2. Calibration of the model**

153   Several strategies for the calibration of PROSPECT have been investigated since its first version.

154 All of the procedures have points in common, such as the adjustment of one or several optical

155 constants (SAC of leaf chemical constituents, refractive index) over the VIS, near infrared and

156 shortwave infrared (SWIR) domains. A standard method consists in determining the optical constants

157 individually or simultaneously at each wavelength by using an iterative procedure (Féret et al., 2008;

158 Li and Wang, 2011). So far, there is no unique method, and adaptations have been proposed to

159   calibrate PROSPECT: Malenovský et al. (2006) adjusted SACs for needle-shaped leaves; Féret et al.

160   (2008) have simultaneously determined the refractive index and SAC of leaf constituents; Chen and

161   Weng (2012) have computed an individual refractive index for each leaf sample. In this section, we

162   provide information about the calibration of PROSPECT-D, including the selection of the calibration

163   dataset, as well as the main steps leading to updated optical constants.

164   **2.1. Available datasets**

165   Six independent datasets collected by several researchers for diverse purposes have been used

166   in this study (Table 1). They share directional-hemispherical reflectance and/or transmittance

167   spectra, and at least two pigments out of three (chlorophylls, carotenoids, and anthocyanins)

168   measured using wet chemistry. The ANGERS dataset includes more than 40 plant species; all the

169   other datasets are monospecies: European hazel (*Corylus avellana* L.) in HAZEL, Norway maple (*Acer*

170   *platanoides* L.) in MAPLE, Virginia creeper (*Parthenocissus quinquefolia* (L.) Planch) in VIRGINIA, and

171   Siberian dogwood (*Cornus alba* L.) in DOGWOOD-1 and -2. Table 1 summarizes the spectral and

172   chemical information available for each dataset. Additional information about the protocols used to

173   conduct the experiments, collect the leaves, measure their optical properties and determine their

174   wet chemistry can be found in (Féret et al., 2008; Gitelson et al., 2009, 2006, 2001; Merzlyak et al.,

175   2008). Note that DOGWOOD-2 does not contain transmittance spectra; that the total chlorophyll

176   content (C_{ab}, expressed in µg cm^{-2}) is available in all datasets; that the total carotenoid content (C_{xc},

177   expressed in µg cm^{-2}) and the total anthocyanin content (C_{anth}, expressed in µg cm^{-2}) have not been

178   determined in HAZEL and ANGERS, respectively. Finally, the 400-780 nm spectral range used for the

179   calibration of the pigment content is common to all datasets except DOGWOOD-1.

180

181   **Table 1.** Description of the leaf datasets used in this study. * The ANGER dataset is available online http://opticleaf.ipgp.fr/index.php?page=database.

Database	Reference	Spectral range (nm)	Number of leaves	Optical properties	Chlorophyll content C_{ab} (µg cm^{-2})			Carotenoid content C_{xc} (µg cm^{-2})			Anthocyanin content C_{anth} (µg cm^{-2})		
					Mean ± SD	Min	Max	Mean ± SD	Min	Max	Mean ± SD	Min	Max
ANGERS*	1, 2	400-2500	308	R & T	34.41 ± 21.85	0.78	106.70	8.84 ± 5.14	0.00	25.28	N/A	N/A	N/A
VIRGINIA	3, 4	400-800	81	R & T	11.05 ± 14.60	0.09	53.76	2.98 ± 3.06	0.15	12.27	8.63 ± 10.77	0.00	37.50
MAPLE	3, 4, 6	400-780	48	R & T	7.43 ± 7.36	0.14	32.98	5.25 ± 2.37	1.82	10.40	8.75 ± 6.83	1.12	21.66
DOGWOOD-1	3, 4, 5	440-796	20	R & T	4.53 ± 4.84	0.07	15.03	2.96 ± 2.06	0.42	5.71	6.88 ± 5.52	0.40	15.49
HAZEL	3, 4	400-800	13	R & T	26.37 ± 3.55	22.69	34.62	N/A	N/A	N/A	7.13 ± 4.19	0.25	13.61
DOGWOOD-2	6	400-1000	51	R	23.77 ± 7.58	1.53	39.81	5.39 ± 2.26	1.73	10.76	12.71 ± 8.21	1.07	30.23

182   1: Féret et al. (2008); 2: Féret et al. (2011); 3: Merzlyak et al. (2008); 4: Gitelson et al. (2009); 5: Gitelson et al., (2001); 6: Gitelson et al. (2006).

183

184

185 **2.2. Data selection for calibration**

186 The calibration of PROSPECT-D requires the leaf samples to have general properties at a

187 minimal level: *i)* pigment content expressed in the same unit for chlorophylls, carotenoids, and

188 anthocyanins, and *ii)* reflectance and transmittance spectra in the 400-780 nm wavelength range. A

189 challenge to calibrating a high performance leaf optical properties model is the lack of

190 comprehensive datasets meeting these two criteria. Among those available, only VIRGINIA and

191 MAPLE fulfill these conditions. Preliminary calibration tests using part or all of these datasets led to

192 SACs with strong discrepancies and poor performances for the estimation of pigment content.

193 Therefore we considered alternative methods combining different data sources and expanding the

194 pool of available calibration data to fill in the gaps. Féret et al. (2008) exploited the ANGERS dataset

195 to calibrate PROSPECT-4 and -5. It is characterized by a wide range of leaf types and pigment

196 contents, and it proved to be well suited for the determination of the SAC of the chlorophyll and

197 carotenoid pigments. These desirable properties of ANGERS come from the variety of leaf types:

198 while chlorophyll and carotenoids contents are usually highly correlated in mature leaves, ANGERS

199 includes juvenile, stressed and senescent leaves lowering this correlation and allowing the SAC of

200 each of these pigments to be adjusted independently from the others, despite their overlapping

201 domain of absorption. Therefore we took the decision to include ANGERS in the calibration dataset

202 and to estimate the corresponding C_{anth} using a spectral index. To avoid the associated uncertainty

203 leading to errors in the SACs, we combined a subset of ANGERS with a subset of VIRGINIA that

204 included accurate measurements of C_{anth} obtained by wet chemistry (Merzlyak et al., 2008). Leaves

205 from VIRGINIA were collected in a park at Moscow State University; they contained very high levels

206 of anthocyanin and low to moderate levels of chlorophyll and carotenoids; they displayed the

207 maximum range of anthocyanin among all the available datasets. In this section, we first explain how

208 C_{anth} was estimated in ANGERS, and then how we split ANGERS and VIRGINIA into calibration and

209   validation subsets. Finally, we present a sensitivity study intended to analyze the influence of the

210   expected C_{anth} uncertainty in ANGERS on the performances of the model.

211

212   **2.2.a. Estimation of leaf anthocyanin content in ANGERS**

213   Several nondestructive methods to estimate C_{anth} from leaf reflectance have been identified

214   and tested on experimental data for which the anthocyanin content has been measured. These

215   methods included spectral indices and machine learning algorithms such as support vector regression

216   (Gitelson et al., 2001, 2006, 2009; van den Berg and Perkins, 2005; Pfündel et al., 2007). The modified

217   Anthocyanin Reflectance Index ($mARI$) designed by Gitelson et al. (2006) led to the best results

218   when using a leave-one-out cross-validation. This index is defined by:

219

220

$$mARI = \left(R_{green}^{-1} - R_{red\ edge}^{-1} \right) \times R_{NIR} \qquad \text{Eq. 1}$$

221

222   where R_{green} is the mean reflectance between 540 nm and 560 nm, $R_{red\ edge}$ the mean reflectance

223   between 690 nm and 710 nm, and R_{NIR} the mean reflectance between 760 nm and 800 nm. We first

224   studied the relationship between $mARI$ and C_{anth} over the 213 samples for which information about

225   anthocyanins was available, i.e., all datasets of Table 1 with the exception of ANGERS. We found a

226   strong linear relationship for $mARI$ values smaller than 5 (137 samples, R^2 = 0.90, RMSE = 1.18 μg

227   cm^{-2}) and a weak one for $mARI$ values greater than 5 (76 samples, R^2 = 0.37, RMSE = 6.35 μg cm^{-2})

228   (Figure 1). These samples with $mARI < 5$ correspond to mature green, yellow, and reddish/red

229   leaves with C_{anth} values less than 12 μg cm^{-2}. Leaves with C_{anth} values higher than 12 μg cm^{-2} are

230   generally dark red and contain small amounts of chlorophyll. In that case, absorptance between 540

231   nm and 560 nm exceeded 90% and further increases of anthocyanin did not change leaf optical

232   properties. A linear model for anthocyanin estimation (Eq. 2) was then derived from the subset

233   excluding the samples with $mARI > 5$ and $C_{anth} > 12$ μg cm^{-2}.
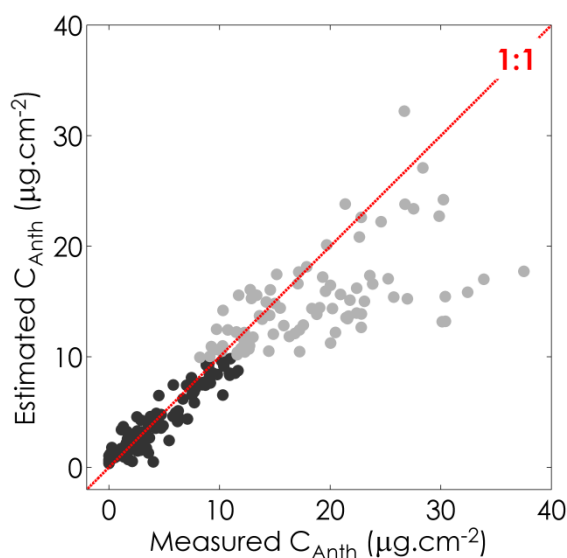
234

$$C_{anth} = 2.11 \times mARI + 0.45 \qquad \text{Eq. 2}$$

235

236   Eq. 2 was applied to the ANGERS dataset to determine C_{anth}. The anthocyanin content ranged

237   from 0 to 17.1 µg cm^{-2}, with a mean value of 1.7 µg cm^{-2}.

238

Figure 1. Relationship between C_{anth} obtained from wet chemistry and C_{anth} estimated from

reflectance data after application of Eq. 2. The black dots correspond to the 137 leaf samples with

$mARI < 5$ (R^2 = 0.90) and the grey dots correspond to the 76 leaf samples with $mARI > 5$ (R^2 =

0.37). Eq. 2 was adjusted only on the black dots.

239   ***2.2.b. Selection of the calibration samples***

240   In order to keep as many samples as possible, we decided to build a calibration dataset made of leaf

241   samples selected both in ANGERS and VIRGINIA. The influence of the uncertainty associated to C_{anth}

242   in ANGERS is expected to be mitigated by the accuracy of C_{anth} in VIRGINIA.

243   In VIRGINIA we identified samples characterized by low C_{ab} ($< 20\ \mu g\ cm^{-2}$) and C_{xc} ($< 5\ \mu g\ cm^{-2}$)

244   in order to decrease the combined influence of the pigments on leaf optical properties, but also to

245   minimize the correlation among pigments. It should allow capturing the influence of anthocyanins

246   independently from the other pigments. We randomly selected 20 samples, leaving a total of 61

247   samples of VIRGINIA for the validation.

248   In ANGERS we discarded at first 14 atypical samples, the spectral behavior of which was

249   incompatible with PROSPECT assumptions. For example, we removed samples collected on

250   *Eucalyptus gunnii* and *Cornus alba*, the overall reflectance of which was very high in the VIS because

251   of the presence of wax (Barry and Newnham, 2012); and three samples of *Schefflera arboricola*

252   displaying uncharacteristic optical properties in the blue (400-450 nm). We also removed samples

253   with $mARI > 5$ as the uncertainty associated to C_{anth} was particularly high (Figure 1). Finally we

254   eliminated leaf samples that had little influence on the calibrated SACs. For that purpose we

255   determined a reference SAC for each pigment using the 314 preselected leaf samples (20 from

256   VIRGINIA and 294 from ANGERS). The ANGERS samples inducing changes in the SACs higher than 5%

257   between 425 nm and 475 nm were kept in the calibration datasets, the others were transferred to

258   the validation dataset.

259   In total, a dataset named CALIBRATION and combining subsets of ANGERS (144 samples) and

260   VIRGINIA (20 samples) was used for the calibration phase.

261   ***2.2.c. Sensitivity of the calibration to the uncertainty associated with C_{anth} in ANGERS***

262   As abovementioned, determining C_{anth} with a spectral index like $mARI$ leads to uncertainty likely to

263   impact the quality of the calibration. We performed a sensitivity analysis with the aim of

264   understanding the influence of this uncertainty on the SACs and on the overall performances of the

265   model. It consisted in adding a Gaussian noise (σ = 1.18 μg cm⁻2) to C_{anth} in ANGERS prior to the

266   calibration and validation procedure. We repeated the operation 50 times.

267

268   **2.3. Selection of the refractive index**

269   PROSPECT is based on the generalized plate model proposed by (Allen et al., 1970, 1969). A

270   plant leaf is modeled as a pile of elementary layers characterized by an absorption coefficient and a

271   refractive index provided at a given wavelength. In the first version of the model, Jacquemoud and

272   Baret (1990) used an albino maize leaf to obtain an experimental spectrum of the refractive index for

273   the elementary layers. le Maire et al. (2004) and Féret et al. (2008) adopted a new strategy based on

274   numerical optimization to determine the optical constants of PROSPECT at the same time. Their

275   refractive index performed slightly better than the previous versions at estimating leaf chemical

276   constituents, but the strong spectral variations observed in the visible wavelengths induced small

277   artifacts in the optical properties of leaves displaying high pigment content. Stuckens et al. (2009)

278   also adjusted a unique refractive index for all leaves.

279   Attempts to obtain a unique refractive index spectrum for all leaves are actually unfounded

280   and inconsistent with the Kramers-Kronig relations that state that the real (refractive index) and

281   imaginary (absorption coefficient) parts of the complex refractive index of a medium are physically

282   linked (Lucarini et al., 2005). These relations allow direct computation of the refractive index of a

283   medium based on its absorption properties on an extended spectral domain. Chen and Weng (2012)

284   used the Kramers-Kronig relations to derive an effective refractive index adjusted to each leaf

285   sample, obtaining very promising results. However, leaf chemical and spectral databases are often

286   incomplete; in particular they cover a limited range of the electromagnetic spectrum, so such a

287   method is impracticable. As a consequence we considered the refractive index to be independent of

288   the leaf sample in this study, but changed strategy compared to PROSPECT-5 in order to avoid the

289   abovementioned artifacts resulting from numerical optimization. Two options were tested: 1) using

290   the refractive index imbedded in PROSPECT-3, and 2) taking the average refractive index derived

291   from minimum and maximum values computed by Chen and Weng (2012) and corresponding to the

292   boundaries of the grey area in Figure 2. The spectra displayed in Figure 2 strongly differ in shape in

293   the VIS: the overall profile of the refractive indices computed by Chen and Weng (2012) is quite

294   similar to that measured for pure liquid water (Hale and Querry, 1973), gradually decreasing from the

295   visible to the infrared, whereas the indices in PROSPECT-3 and -5 are very much alike in the near and

296   shortwave infrared (1000-2500 nm) and show a steeper decrease. Divergence between the refractive

297   index derived from Chen and Weng (2012) and those used in PROSPECT-3 and -5 strongly increases

298   with wavelength. We performed the full calibration of PROSPECT (including optimal adjustment of

299   SAC as described in Section 2.2.b) with each refractive index.

300
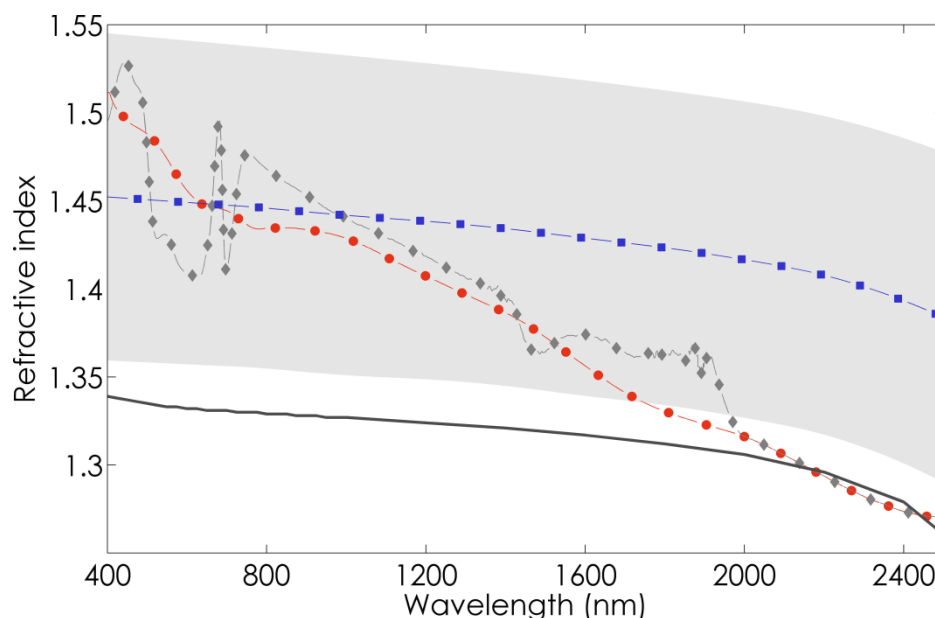
Figure 2. Comparison of the refractive index used in PROSPECT-3 (red dots), PROSPECT-5 (grey

diamonds) and corresponding to the mean refractive index proposed by (Chen and Weng, 2012)

(blue squares). The grey area corresponds to the range of variation of the refractive index proposed

by Chen and Weng, (2012); the plain grey line corresponds to the refractive index for pure liquid

water (Hale and Querry, 1973).

301

302   **2.4. Optimal adjustment of the specific absorption coefficients**

303   The adjustment of the SAC for each group of pigments is based on numerical optimization

304   routines applied to experimental data. As in PROSPECT-5 we assumed that the chlorophyll *a:b* ratio

305   was constant and we combined carotenes and xanthophylls in the carotenoid group. Similarly

306   anthocyanins were assumed to include all types of anthocyanins contributing to light absorption in

307   the VIS. Given the well-known sensitivity of the anthocyanin absorption properties to pH, which is

308   due to a reversible structural change that occurs in the C ring of the molecule, this hypothesis may be

14

309   incorrect in certain situations. However, environment inside a vacuole is generally slightly acid, with

310   pH values reported to fall within the range of 5.0 to 6.0 pH units, with a mean pH of 5.5 (Mathieu et

311   al., 1989; Martinière et al., 2013).

312   Solved SAC values were constrained to be positive. To prevent erroneous absorption

313   assignments, the wavelength domains were narrowed to 400-750 nm for chlorophylls, 400-560 nm

314   for carotenoids, and 400-660 nm for anthocyanins. These ranges are broader than *in vitro* due to the

315   detour effect: the lengthening of the optical path-length within the leaf results in substantial

316   flattening of the absorption spectrum *in vivo* (e.g., Rühle and Wild, 1979; Fukshansky et al., 1993).

317   The calibration followed a two-steps algorithm described in Féret et al. (2008). First, we

318   determined the structure parameter N_j of each leaf j in the calibration datasets on the basis of an

319   iterative optimization: N_j was estimated based on a multivariate iterative optimization,

320   simultaneously with three absorption coefficients using reflectance and transmittance values

321   measured at three wavelengths corresponding to the minimum absorptance (λ_1), maximum

322   reflectance (λ_2), and maximum transmittance (λ_3) of the leaf. These values are generally located on

323   the NIR plateau. The iterative optimization was performed using the merit function:

324

$$M_{leafN}\left(N_j, k(\lambda_1), k(\lambda_2), k(\lambda_3)\right)$$
$$= \sum_{l=1}^{3}\left(R_{meas,j}(\lambda_l) - R_{mod}\left(N_j, k(\lambda_l)\right)\right)^2 + \left(T_{meas,j}(\lambda_l) - T_{mod}\left(N_j, k(\lambda_l)\right)\right)^2 \qquad \text{Eq. 3}$$

325

326   with $R_{meas,j}(\lambda_l)$ and $T_{meas,j}(\lambda_l)$ the measured reflectance and transmittance of leaf j at the

327   wavelength λ_l, R_{mod} and T_{mod} the modeled values, and $k(\lambda)$ the absorption coefficient of a

328   compact layer at the wavelength λ, which is adjusted simultaneously with N_j. In Eq. 3, $k(\lambda)$ is not

329   decomposed into specific absorption of the different chemical constituents. This step occurs in the

330   NIR where pigments have little if any influence, so $k(\lambda)$ is primarily affected by water absorption.

331   The SAC to be calibrated were then computed by inverting PROSPECT on the $n = 164$ leaves of the

332   calibration dataset. We minimized the merit function J at each wavelength:

333

$$J\left(\left\{K_{spe,i}(\lambda)\right\}_{i=1:n}\right)$$
$$= \sum_{j=1}^{n}\left(R_{meas,j}(\lambda) - R_{mod,j}\left(N_j, k(\lambda)\right)\right)^2 \qquad \text{Eq. 4}$$
$$+ \left(T_{meas,j}(\lambda) - T_{mod,j}\left(N_j, k(\lambda)\right)\right)^2$$

334

335   where

336

$$k(\lambda) = \frac{\sum_i K_{spe,i}(\lambda) \times C_{i,j}}{N_j} \qquad \text{Eq. 5}$$

337

338    $k(\lambda)$ is the absorption coefficient of a compact layer at the wavelength λ, $K_{spe,i}(\lambda)$ is the SAC

339   of constituent i, $C_{i,j}$ is the corresponding content for leaf j, N_j is the leaf structure parameter of leaf

340   j, and n corresponds to the number of biochemical constituents for which the SACs are

341   simultaneously calibrated.

342

343   **3. Validation: datasets and criteria for the comparison of model performances**

344   We performed model inversions on the validation dataset with PROSPECT-D, as well as

345   PROSPECT-3 and -5. The performances of the different versions of the model were compared in

346   terms of pigment content estimation and leaf spectra fit. The validation was performed using all leaf

347   samples after exclusion of the calibration samples.

348   PROSPECT was inverted on the validation dataset using an iterative method for optimization. It

349   consists in finding the best combination of leaf chemical and structural parameters that minimizes

350   the merit function:

351

352

$$M_{inv}\left(N,\{C_i\}_{i=1:p}\right)$$
$$= \sum_{\lambda=1}^{n_\lambda} \left(R_{meas,\lambda} - R_{mod,\lambda}\left(N,\{C_i\}_{i=1:p}\right)\right)^2 \qquad \text{Eq. 6}$$
$$+ \left(T_{meas,\lambda} - T_{mod,\lambda}\left(N,\{C_i\}_{i=1:p}\right)\right)^2$$

353

354 with n_λ the number of available spectral bands, N the leaf structure parameter, C_i the content of

355 constituent i, and p the number of leaf biochemical constituents. In this study, we simultaneously

356 estimated the six input parameters of PROSPECT: pigments (C_{ab}, C_{xc}, C_{anth}), equivalent water

357 thickness (EWT), leaf mass per area (LMA) and leaf structure parameter (N).

358 In essence, candidate sets of these parameters are iteratively input in forward mode and the

359 resulting modeled reflectance and/or transmittance spectra compared against the measured ones;

360 the parameter are revised until the minimum value of the merit function is found. When the

361 assumptions of the model are not met, for example if a pigment is not taken into account, or if the

362 SACs are incorrect, the inversion will converge towards a suboptimal solution, inducing errors in the

363 estimation of the parameters. This situation occurs when we try to invert PROSPECT-3 on yellowing

364 leaves; C_{ab} is overestimated to compensate for the absorption of C_{xc}.

365 The root mean square error (*RMSE* expressed in µg cm^{-2}) can be computed to appraise the

366 difference between the measured and estimated pigment content:

367

$$RMSE = \sqrt{\frac{\sum_{j=1}^{n}\left(X_{meas,j} - X_{mod,j}\right)^2}{n}} \qquad \text{Eq. 7}$$

368

369 where $X_{meas,j}$ are the measured values and $X_{mod,j}$ are the values estimated by model inversion for

370 leaf j. As for the quality of the fit, it is appraised by the spectral RMSE which calculates the difference

371 between the measured and simulated reflectance and transmittance spectra on a wavelength-by-

372 wavelength basis.

373

374 **4. Results**

17

4.1. Selection of a calibration dataset

375

376   Figure 3 shows the pigment distribution corresponding to the calibration and validation

377   samples in ANGERS and VIRGINIA: note that the calibration samples display low to moderate C_{ab} and

378   C_{xc} values, whereas the validation samples encompasses significantly broader pigment contents. The

379   calibration samples with high C_{anth} come from VIRGINIA, for reasons explained earlier.

380
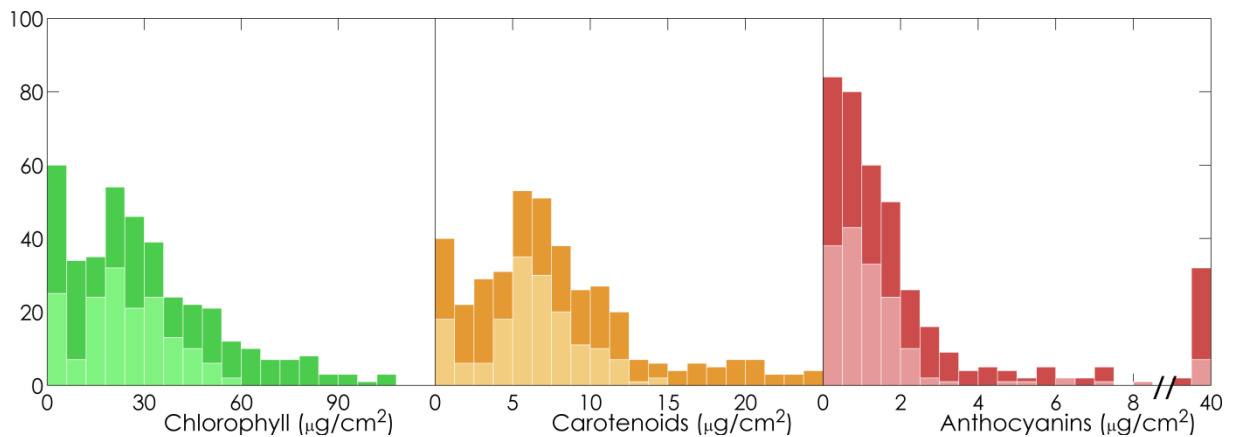
Figure 3. Stacked distribution of pigment content for the calibration and validation samples selected from ANGERS and VIRGINIA. Light colors: calibration (144 samples from ANGERS, 20 Samples from VIRGINIA); dark colors: validation (164 samples from ANGERS, 61 samples from VIRGINIA).

381

4.2. Selection of the refractive index

382

383   The refractive index spectra displayed in Figure 2 provide advantages and disadvantages in

384   terms of model accuracy both for the estimation of leaf chemistry and the simulation of leaf optical

385   properties. We performed calibrations of PROSPECT-D as detailed in Section 3, using either the

386   refractive index of PROSPECT-3 and the one derived by Chen and Weng (2012). Then we inverted the

387   two versions of the model on ANGERS, the only dataset covering the SWIR as well as including

388   measurements of EWT and LMA. Overall the performances obtained for pigment retrieval and

389   simulation of leaf optics were similar in the VIS. For water and dry matter, results were also very

390   similar. Simulated leaf reflectance and transmittance spectra also exhibited very slight differences in

391   the VIS, while they were noticeable in the NIR and SWIR. This is illustrated by Figure 4 that displays

392   the spectral RMSE calculated between measured and simulated leaf spectra for ANGERS. The

393   reflectances are comparable, with slightly higher RMSE obtained with the refractive index derived

394   from Chen and Weng (2012) between 1500 nm and 1900 nm; there are higher discrepancies in the

395   transmittances. Based on these results, we assigned the refractive index used in PROSPECT-3 to

396   PROSPECT-D.

397
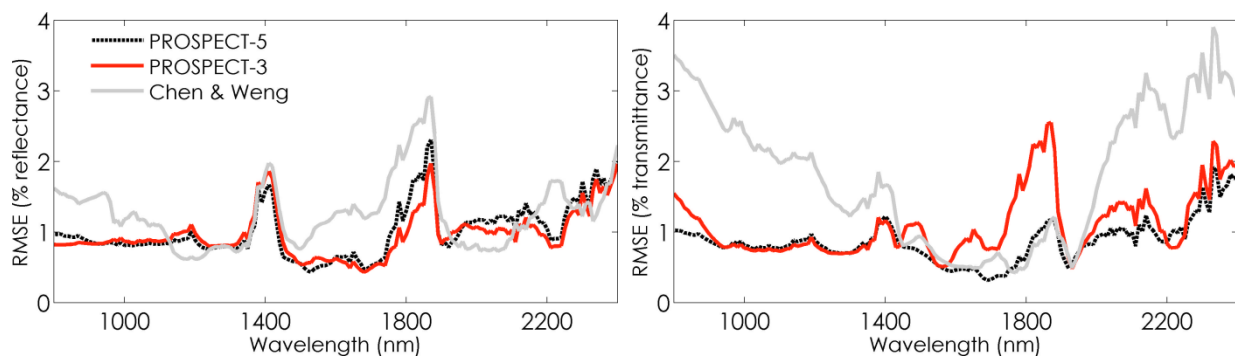
Figure 4. Spectral RMSE between measured leaf optics and simulated reflectance (left), and

transmittance (right) obtained after model inversion with the refractive index used in PROSPECT-5

(black dotted line), PROSPECT-3 (red), and derived from Chen and Weng (2012) (light grey).

398

399   **4.3. Adjustment of the specific absorption coefficients**

400   Figure 5 displays the SACs of pigment in PROSPECT-5 and PROSPECT-D. The differences

401   between the two models are minor for chlorophylls and carotenoids beyond 450 nm. However,

402   noticeable differences can be observed for carotenoids between 400 nm and 450 nm: compared to

403   PROSEPCT-D, the SAC of C_{xc} sharply increases towards the ultraviolet (UV) domain in PROSPECT-5,

404   possibly due to the presence of flavonoids in the calibration samples. This augmentation is

405   compensated by a slight decrease of the SACs of C_{ab} and C_{anth}. The SAC of anthocyanins shows a

406   strong absorption between 450 nm and 650 nm, that peaks at about 550 nm. This result is in

407   agreement with the absorption spectra reported in the literature (Dougall and Baker, 2008; Peters

408   and Noble, 2014). The broadness of the absorption peak may be caused by calibration artifacts

409   related to residual correlations between the pigments.

410
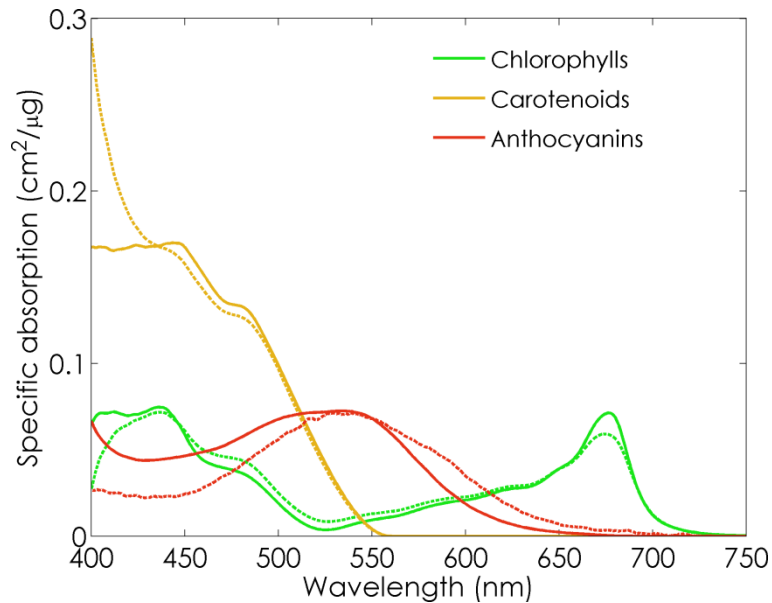
Figure 5. Specific absorption coefficients of chlorophylls (green), carotenoids (orange), and

anthocyanins (red). The solids line correspond to the SAC of all the pigments in PROSPECT-D, the

dashed lines to the SAC of chlorophylls and carotenoids in PROSPECT-5, and to the SAC of

anthocyanins measured by Peters and Noble (2014) using thin layer chromatography.

411

412   **4.4. Validation of model performances**

413   4.4.a. Estimation of leaf pigment by PROSPECT inversion

414   C_{ab}, C_{xc} and C_{anth} have been estimated by inversion of PROSPECT-D on a dataset hereafter

415   called VALIDATION. It gathered all experimental datasets (Table 1) except DOGWOOD-2 which did

416   not contain transmittance spectra. ANGERS was also excluded for anthocyanins since C_{anth} has been

417   indirectly estimated using a spectral index.

418   Table 2 compares the performances of PROSPECT-3, -5 and -D for pigment estimation in terms

419   of RMSE. One can note a markedly improvement of C_{xc} estimation by PROSPECT-D for all datasets. In

420   ANGERS, which mainly contain green leaves, PROSPECT-5 and PROSPECT-D perform similarly at

421   estimating C_{ab}, with a slight increase of RMSE obtained with PROSPECT-D. It can be explained by the

422   fact that these samples correspond to calibration samples in PROSPECT-5. PROSPECT-D surpasses the

423   previous versions of the model for all datasets other than ANGERS. Importantly, the new model is

424   able to accurately estimate C_{xc} even in anthocyanic leaves, which has been problematic for other

425   techniques.

426

427   **Table 2.** RMSE (µg cm^{-2}) of the estimation of leaf pigment content using PROSPECT-3 (P-3),

428   PROSPECT-5 (P-5), and PROSPECT-D (P-D) inversion. The bold font for numbers indicates the lowest

429   values.

| Database	C_{ab}			C_{xc}		C_{anth}
	P-3	P-5	P-D	P-5	P-D	P-D
CALIBRATION	6.84	3.69	**3.43**	6.69	**1.31**	1.74
ANGERS (VAL)	11.07	**6.71**	7.07	6.90	**3.81**	3.22
MAPLE	15.54	7.85	**3.28**	17.28	**2.23**	2.34
VIRGINIA (VAL)	14.38	7.74	**2.95**	17.41	**1.19**	4.54
DOGWOOD-1	14.94	7.90	**3.12**	18.07	**1.21**	2.24
HAZEL	20.88	9.67	**2.36**	n.a.	**n.a.**	2.82
DOGWOOD-2	37.22	16.51	**6.08**	20.92	**10.92**	14.39
VALIDATION	13.33	7.33	**5.58**	12.67	**3.06**	3.49

430

431   Figure 6 illustrates the differences observed in Tables 2. PROSPECT-3 overestimated C_{ab} for all

432   datasets, even with ANGERS which mainly contained green leaves; this overestimation was reduced

433   when using PROSPECT-5 or PROSPECT-D. The substantial improvement in C_{xc} estimation when using

434   PROSPECT-D is a significant result of this article: overall, the RMSE was divided by four compared to

435   the results obtained with PROSPECT-5. The inversion of PROSPECT-5 on anthocyanin-rich leaves

436   sometimes converged towards the upper bound on C_{xc} (30 µg cm^{-2}). It is likely that this

437   overestimation of carotenoid content results from the strong absorption of light by anthocyanins in

438   the same wavelength range as carotenoids, and this absorption is not properly modeled by

439   PROSPECT-5. In ANGERS, the systematic underestimation of C_{xc} by PROSPECT-5 in leaves containing

440   high amounts of photosynthetic pigments was greatly reduced by PROSPECT-D. The overestimation

21

441   of C_{xc} in anthocyanin-rich leaves was also corrected. The lower performances of PROSPECT-D on

442   DOGWOOD-2 are probably explained by the absence of transmittance spectra. As explained in

443   **Section 4.1**, the samples selected for the calibration dataset in ANGERS were marked out by low to

444   medium pigment content, therefore they were not representative of the full range of variation found

445   in this dataset: nevertheless, this did not prevent us from estimating high pigment content with

446   accuracy. This is explained by slight changes in the optical properties of leaves with high-pigment

447   content when carotenoids increase, due to saturation effects. It also suggests that the physical

448   description used in PROSPECT is correct, as its ability to estimate pigment content goes beyond the

449   range used for calibration. Samples showing underestimated C_{xc} in ANGERS were discarded from the

450   calibration dataset due to unusual optical properties (surface effects) or very high $mARI$.

451

452
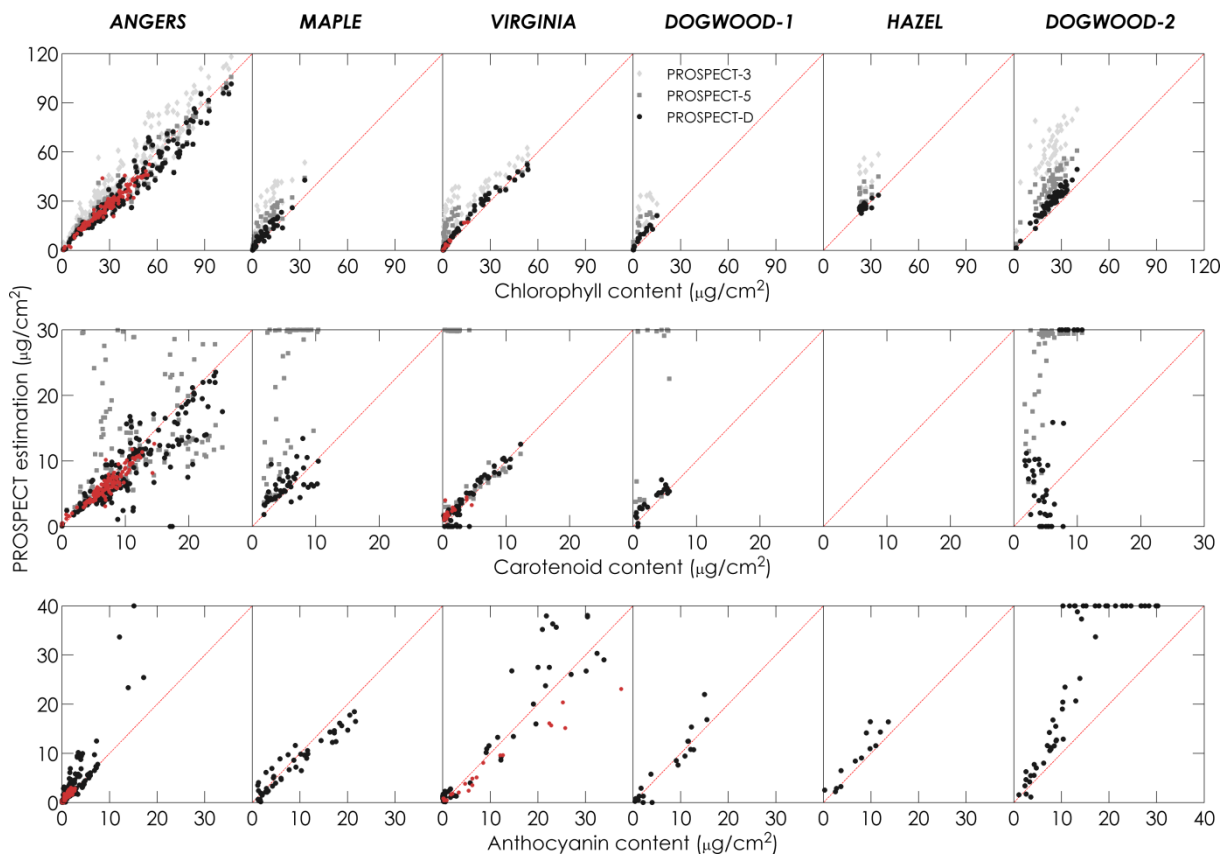
Figure 6. Estimation of pigment content by inversion of three versions of PROSPECT on six datasets

(when relevant). Red dots correspond to calibration samples from ANGERS and VIRGINIA.

453

454   4.4.b. Spectrum reconstruction

455   We compared the spectral RMSE between measured spectra and spectra reconstructed by the

456 last three versions of PROSPECT after model inversion on the VALIDATION dataset (Figure 7). Values

457 obtained with PROSPECT-3 ranged between 2% and 6% over the VIS. This model uses a unique SAC to

458 account for total pigment absorption; therefore it solely applies to healthy green leaves. The

459 dissociation of chlorophylls from carotenoids in PROSPECT-5 explains the strong decrease in RMSE

460 between 400 nm and 500 nm where carotenoids absorb light. However, the discrepancies are still

461 strong between 500 nm and 600 nm where anthocyanins absorb light, and between 650 nm and 750

462 nm, a spectral domain that corresponds to the second absorption peak of chlorophylls. Finally,

463 PROSPECT-D surpassed the previous versions with RMSE ranging between 1% and 2% over the entire

464 VIS.

465
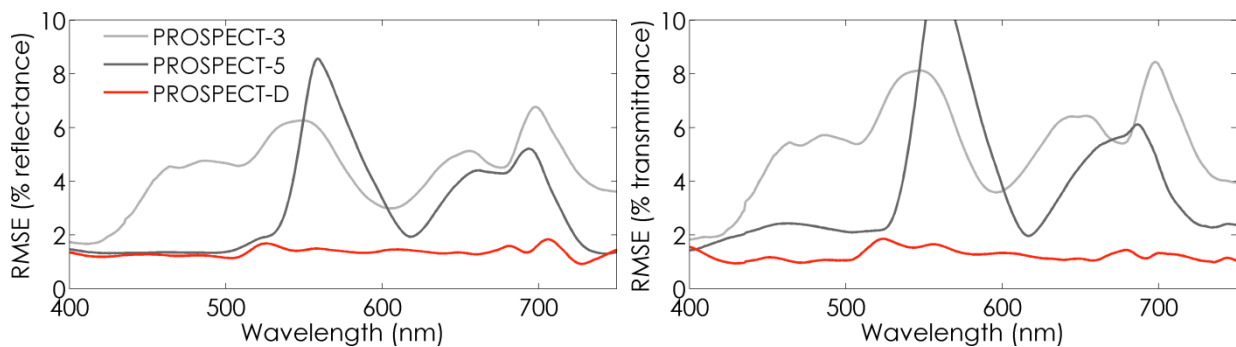
Figure 7. Spectral RMSE between measured and estimated leaf reflectance and transmittance

obtained for the VALIDATION dataset after model inversion using PROSPECT-3, PROSPECT-5, and

PROSPECT-D.

466

467

468

469   **4.5. Sensitivity to the uncertainty associated with C_{anth} in ANGERS**

470   4.5.a. Specific absorption coefficients

471   The addition of noise to C_{anth} in ANGERS influences the calibration of the SACs of PROSPECT, as

472   expected, but the variability is limited to the 400-500 nm wavelength range, especially for

473   anthocyanins. The main difference for this pigment is observed between 500 nm to 600 nm (Figure

474   8).

475
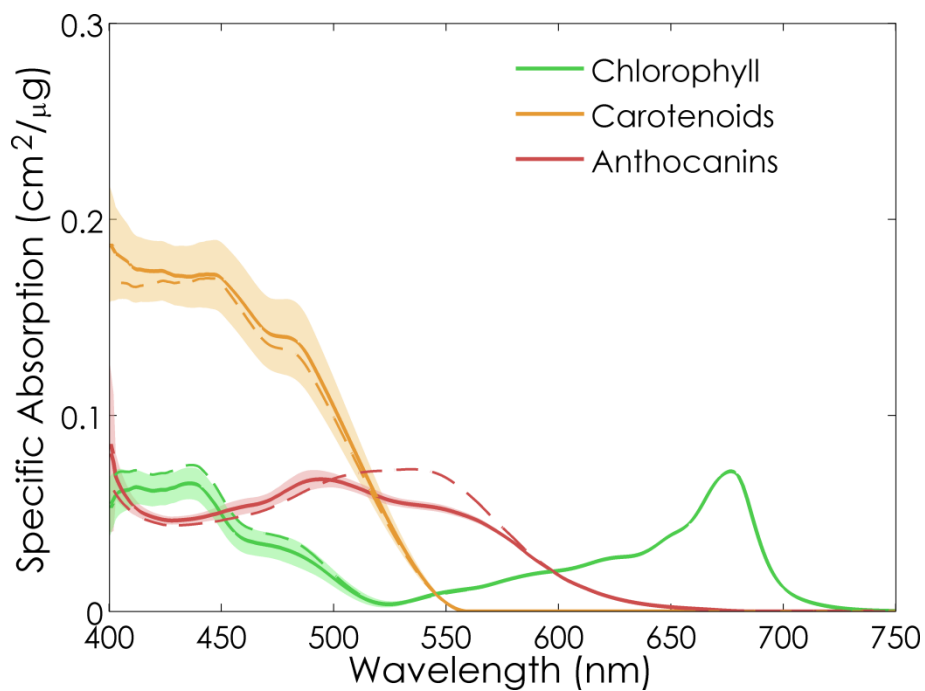
Figure 8. Comparison of the SACs obtained for the three pigments when using C_{anth} values directly

derived from $mARI$ (dashed lines) and when using C_{anth} values with noise added corresponding to

the error of prediction of C_{anth} observed for experimental data (50 repetitions; plain lines and their

envelope correspond to mean value ± 1 standard deviation).

476

477   4.5.b. Estimation of pigment content

478   We estimated pigment content by inverting PROSPECT with the set of SACs derived from noisy C_{anth}.

479   **Erreur ! Source du renvoi introuvable.** summarizes the distributions of RMSE from measured and

480 estimated pigment contents for the validation datasets taken separately and for the VALIDATION

481 dataset that group them together. The uncertainty on C_{anth} has no influence on the estimation of

482 C_{ab}, as the RMSE is close to that obtained when no noise was added to C_{anth}. The influence is higher

483 on the estimation of carotenoids. The version of the model with no noise added to C_{anth}

484 outperformed the versions including noise, particularly for MAPLE. This version also outperformed all

485 noisy versions when focusing on VALIDATION. Finally, the estimation of C_{anth} also performed better

486 when no noise was added to the ANGERS calibration samples, except for MAPLE, which performs a

487 little less now. However as for C_{xc}, the results obtained with VALIDATION showed better estimation

488 of C_{anth} when no noise was added. These results validate the calibration of PROSPECT-D with C_{anth}

489 determined using a spectral index. Moreover, the slight decrease in performances for the estimation

490 of C_{anth} and C_{xc} when adding noise to C_{anth} suggests that the estimated values obtained for C_{anth}

491 in ANGERS may show lower uncertainty than expected based on the experimental data available.

492
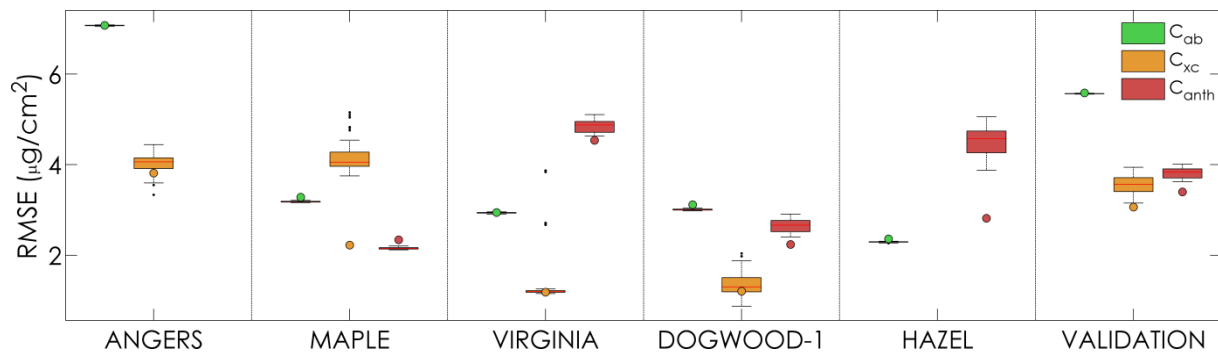
Figure 9. Distribution of the RMSE between measured and estimated pigment content after adding noise to the values of C_{anth} of ANGERS used for calibration of PROSPECT and inversion of the model based on the SACs displayed in Figure 8. Colored dots correspond to the RMSE obtained when no noise is added to C_{anth} in ANGERS.

493

494 4.5.c. Simulation of leaf optical properties

495   The accuracy of reflectance and transmittance reconstruction is displayed in Figure 10. The spectra

496   simulated by PROSPECT-D show very minor differences whatever noise was added to C_{anth} or not.

497   These results confirm that despite missing values and indirect estimation of C_{anth} for ANGERS,

498   PROSPECT-D provides stable results in terms of calibrated SACs as well as model performance both in

499   direct and inverse modes.

500
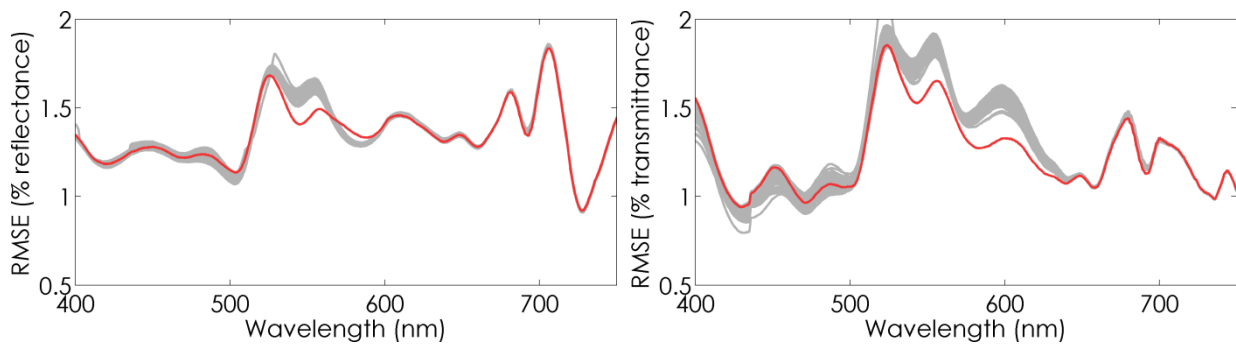
Figure 10. Spectral RMSE between measured and estimated leaf reflectance and transmittance obtained for the VALIDATION dataset after model inversion using PROSPECT-D calibrated with (grey lines) and without (red lines) uncertainty added to C_{anth}.

501

502   **5. Discussion**

503   **5.1. Specific absorption coefficients**

504   As stated earlier, the SAC of anthocyanins obtained after the calibration phase (Figure 5)

505   displayed a broad absorption peak centered on 550 nm. The overall profile agrees well with the

506   spectra obtained in previous studies (Gitelson et al., 2001; Peters and Noble, 2014). We compared

507   this SAC with absorption spectra of pure cyanidin-3-glucoside (C3G), measured in the lab for

508   different pH (Fossen et al., 1998). C3G is also the most common anthocyanin in leaves (Harborne and

509   Williams, 1998). The SACs derived from a model generally do not match data published in the

510   literature for *in vitro* dissolved pigments. Several causes may explain such a discrepancy. First,

511   radiative transfer model are imperfect: for instance, a two-layer model taking into account the

512   asymmetry of leaf anatomy and chemical content in Dicots may improve the determination of the

513   SACs. Moreover, the calibration of these models is based on experimental data which may be not

514   optimal in terms of sampling, despite our efforts to provide the best experimental datasets. Second,

515   molecules *in vivo* are linked to their environment, which may induce shifts in their SACs: this is the

516   case for chlorophylls with proteins, or anthocyanins with the pH or temperature (Figueiredo et al.,

517   1999; Yabuya et al., 1999; Boulton, 2001). Thirdly, while the model assumes stable compositions and

518   absorption spectra for chlorophylls, carotenoids and anthocyanins, in reality these are families of

519   pigments containing between two and hundreds of molecules, with as many variations in their

520   particular absorption spectra. Subtle changes in anthocyanin composition, chlorophyll *a:b* ratio, or

521   induced by the xanthophyll cycle may result in variations in leaf reflectance and transmittance that

522   are detectable but not interpretable by PROSPECT. Finally, as explained earlier, internal multiple

523   scattering (detour effect) and distributional errors (sieve effect) may also explain part of the

524   discrepancies observed between *in vivo* and *in vitro* SACs. **Figure 11**shows the profile of the SAC of

525   anthocyanins: it is intermediate between the absorption coefficient measured for C3G at pH 1 and

526   pH 8.1 in the main absorption domain of this constituent. The increasing absorption closer to the UV-

527   A may be explained by the presence of flavonols in some leaves: these molecules, which are

528   biosynthetically associated with anthocyanins in plant secondary metabolism, are also optically

529   active in this domain. Therefore, it is likely that flavonols contribute to the anthocyanin SAC spectrum

530   (Solovchenko et al., 2001). The improvement of C_{xc} estimation accuracy upon incorporation of

531   anthocyanins into PROSPECT-D may stem from the inherent correlation between anthocyanin and

532   flavonoid content.

533
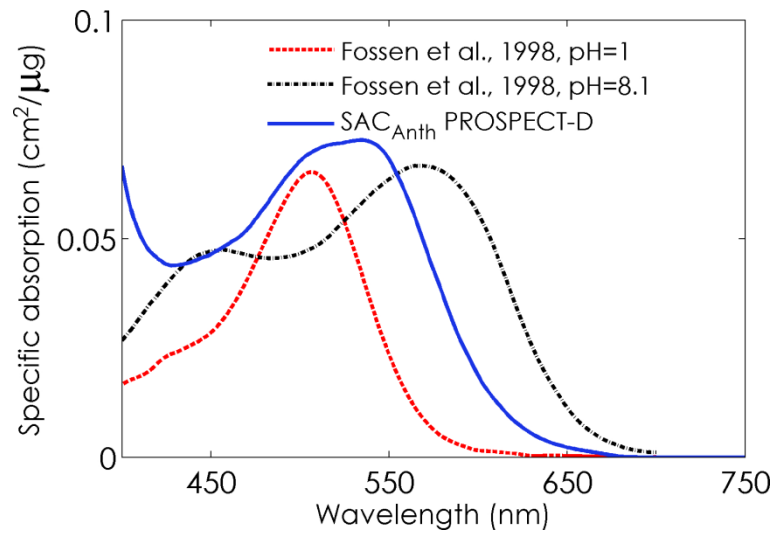
Figure 11. Comparison of the SAC corresponding to anthocyanins derived from PROSPECT-D calibration (cm^2 μg^{-1}) and the absorption of pure Cyanidin 3-glucoside at pH 1 and 8.1 (unitless) (after Fossen et al., 1998).

534

535   The SAC of carotenoids above 450 nm is very similar in PROSPECT-5 and PROSPECT-D. However

536   the estimation of C_{xc} is substantially improved in the latter, which highlights the high sensitivity of

537   PROSPECT to very small changes of the SAC, as well as the importance of incorporating anthocyanins

538   into the model even for leaves with low content. This improvement in the estimation of C_{xc} was not

539   explained by the differences observed between 400 nm and 450nm: when using all the ANGERS

540   dataset for calibration, the SAC calibrated for C_{xc} showed very similar profile as in PROSPECT-5, but

541   the improvement in the estimation of C_{xc} was still observed.

542

543   **5.2. Illustration of the improved simulation of leaf optical properties**

544   To illustrate the ability of PROSPECT-D to simulate leaf optical properties we selected some

545   samples including senescent and reddish leaves (Figure 12). In some cases, the fit is poor: the

546   reflectance spectrum of *Eucalyptus gunnii* is very high compared to that of other leaves, probably

547   due to the presence of wax at the leaf surface, a layer that is not accounted for in PROSPECT (Figure

548   12h). Barry and Newnham (2012) already pointed out an incorrect assessment of carotenoid content

549   in *Eucapyptus globulus* and *Eucapyptus nitens leaves*. The development of PROSPECT-D partly

550   answers these limitations, but further efforts will be needed to include specular reflection (Bousquet

551   et al., 2005; Comar et al., 2014; Jay et al., 2016).

552
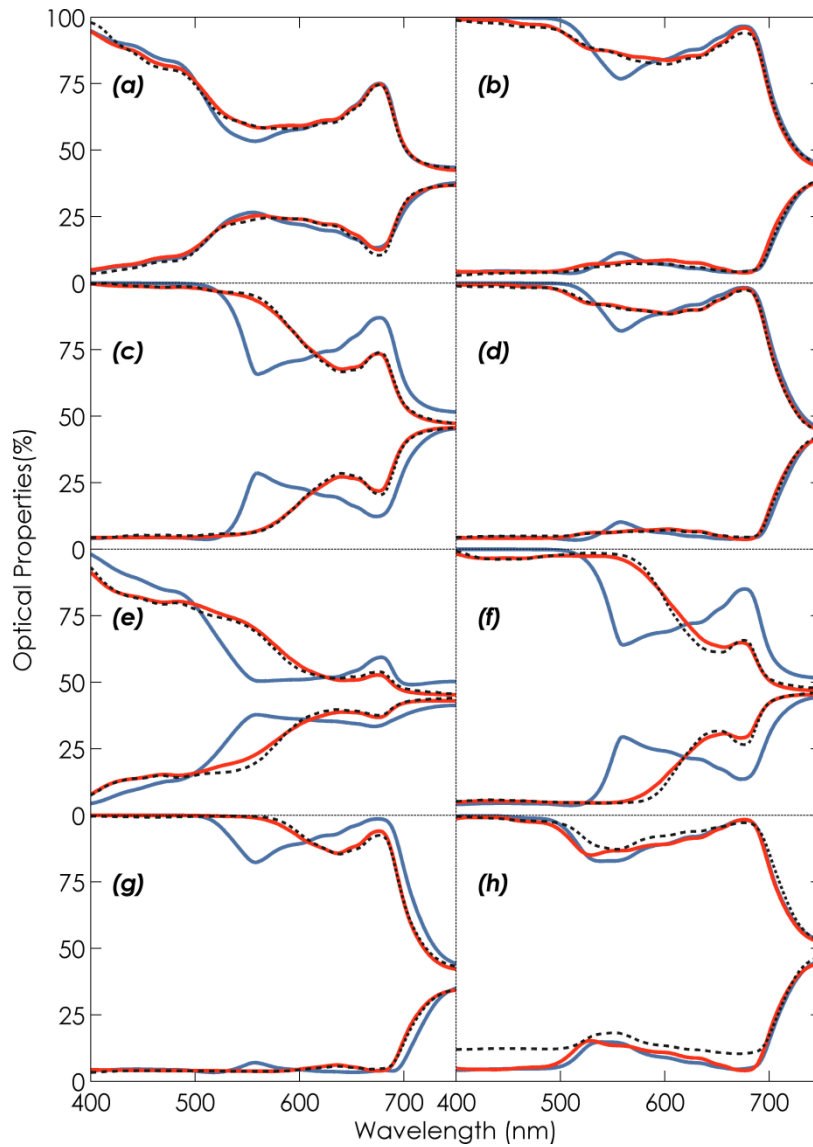
Figure 12. Measured (black dotted line) versus simulated (blue line for PROSPECT-5 and red line for

PROSPECT-D) reflectance (lower spectra) and transmittance (upper spectra). (a-b) *Acer*

pseudoplatanus L., (c) *Acer platanoides* L., (d) *Corylus avellana* L., (e-f) *Parthenocissus quinquefolia*

(L.) Planch., (g) *Corylus maxima 'Purpurea'*, and (h) *Eucalyptus gunnii*. Samples (b-e-f) show non-

senescent anthocyanic leaves, while samples (a-c-d-g) show anthocyanic senescent leaves.

553

554 **6. Conclusion**

555 We introduced a new, physically-based model called PROSPECT-D which, for the first time,

556 includes the three main families of leaf pigments as independent constituents: chlorophylls,

557 carotenoids, and anthocyanins. PROSPECT-D outperformed the previous versions of the model, both

558 for the estimation of leaf chemical constituents and the simulation of leaf optical properties, on

559 datasets encompassing a broad range of growth conditions and stages. Inversion of PROSPECT-D

560 showed improved estimation of pigment content, especially carotenoid content. These results

561 demonstrate the ability of this new model to simulate optical properties during the lifespan of the

562 leaf and for a new range of conditions, including juvenile and senescent stages, as well as

563 environmental stresses.

564 We studied the influence of the uncertainty corresponding to the values of C_{anth} from

565 ANGERS used for the calibration of PROSPECT-D. Our results showed that this uncertainty has little to

566 no impact on the calibration, and on the performances of the model in terms of pigment prediction

567 accuracy, as well as in modeling of leaf optics.

568 The availability of this model has strong implications for vegetation modeling both at leaf and

569 canopy scales. At the leaf scale, PROSPECT-D will allow to perform sensitivity analyses focused on

570 anthocyanins, and to design new vegetation indices dedicated to specific pigments and less sensitive

571 to other ones. The linkage of PROSPECT-D with canopy reflectance models such as SAIL (e.g.,

572 Jacquemoud et al., 2009) or DART (Hernández-Clemente et al., 2012; Gastellu-Etchegorry et al.,

573 2015) will allow simulations of vegetation types that could not be reproduced before. Applications

574 for stress and senescence detection will directly take advantage of such improvements. Finally

575 PROSPECT-D is a powerful tool for determining the potential of operational multispectral satellites

576 (Sentinel-2, LandSat-8, WorldView-3) and future hyperspectral missions (EnMAP, Hyspiri, HYPXIM)

577 for fine detection of leaf pigments.

578

591

References

593   Allen, W.A., Gausman, H.W., Richardson, A.J., 1970. Mean effective optical constants of cotton
594   leaves. J. Opt. Soc. Am. 60, 542–547. doi:10.1364/JOSA.60.000542
595   Allen, W.A., Gausman, H.W., Richardson, A.J., Thomas, J.R., 1969. Interaction of isotropic light with a
596   compact plant leaf. J. Opt. Soc. Am. 59, 1376–1379. doi:10.1364/JOSA.59.001376
597   Asner, G.P., Anderson, C.B., Martin, R.E., Tupayachi, R., Knapp, D.E., Sinca, F., 2015a. Landscape
598   biogeochemistry reflected in shifting distributions of chemical traits in the Amazon forest
599   canopy. Nat. Geosci. 8, 567–573. doi:10.1038/ngeo2443
600   Asner, G.P., Martin, R.E., 2009. Airborne spectranomics: Mapping canopy chemical and taxonomic
601   diversity in tropical forests. Front. Ecol. Environ. 7, 269–276. doi:10.1890/070152
602   Asner, G.P., Martin, R.E., Anderson, C.B., Knapp, D.E., 2015b. Quantifying forest canopy traits:
603   Imaging spectroscopy versus field survey. Remote Sens. Environ. 158, 15–27.
604   doi:10.1016/j.rse.2014.11.011
605   Atzberger, C., Guérif, M., Baret, F., Werner, W., 2010. Comparative analysis of three chemometric
606   techniques for the spectroradiometric assessment of canopy chlorophyll content in winter
607   wheat. Comput. Electron. Agric. 73, 165–173. doi:10.1016/j.compag.2010.05.006
608   Barry, K., Newnham, G., 2012. Quantification of chlorophyll and carotenoid pigments in eucalyptus
609   foliage with the radiative transfer model PROSPECT 5 is affected by anthocyanin and
610   epicuticular waxes., in: Proc. Geospatial Science Research 2 Symposium, GSR 2012,
611   Melbourne, Australia, December 10-12, 2012.
612   Blackburn, G.A., 2007. Hyperspectral remote sensing of plant pigments. J. Exp. Bot. 58, 855–867.
613   doi:10.1093/jxb/erl123

614   Boulton, R., 2001. The copigmentation of anthocyanins and its role in the color of red wine: A critical
615   review. Am. J. Enol. Vitic. 52, 67–87.
616   Bousquet, L., Lachérade, S., Jacquemoud, S., Moya, I., 2005. Leaf BRDF measurements and model for
617   specular and diffuse components differentiation. Remote Sens. Environ. 98, 201–211.
618   doi:10.1016/j.rse.2005.07.005
619   Britton, G., Liaaen-Jensen, S., Pfander, H. (Eds.), 2004. Carotenoids. Birkhäuser Basel, Basel.
620   Brockington, S.F., Walker, R.H., Glover, B.J., Soltis, P.S., Soltis, D.E., 2011. Complex pigment evolution
621   in the Caryophyllales: Research review. New Phytol. 190, 854–864. doi:10.1111/j.1469-
622   8137.2011.03687.x
623   Chappelle, E.W., Kim, M.S., McMurtrey, J.E., 1992. Ratio analysis of reflectance spectra (RARS): An
624   algorithm for the remote estimation of the concentrations of chlorophyll A, chlorophyll B,
625   and carotenoids in soybean leaves. Remote Sens. Environ. 39, 239–247. doi:10.1016/0034-
626   4257(92)90089-3
627   Chen, M., Weng, F., 2012. Kramers-Kronig analysis of leaf refractive index with the PROSPECT leaf
628   optical property model: K-K analysis of leaf refractive index. J. Geophys. Res. Atmospheres
629   117, D18106n. doi:10.1029/2012JD017477
630   Comar, A., Baret, F., Obein, G., Simonot, L., Meneveaux, D., Viénot, F., de Solan, B., 2014. ACT: A leaf
631   BRDF model taking into account the azimuthal anisotropy of monocotyledonous leaf surface.
632   Remote Sens. Environ. 143, 112–121. doi:10.1016/j.rse.2013.12.006
633   Davies, K., 2004. Plant pigments and their manipulation. Blackwell ; CRC, Oxford; Boca Raton.
634   Di Vittorio, A.V., 2009. Enhancing a leaf radiative transfer model to estimate concentrations and in
635   vivo specific absorption coefficients of total carotenoids and chlorophylls a and b from single-
636   needle reflectance and transmittance. Remote Sens. Environ. 113, 1948–1966.
637   doi:10.1016/j.rse.2009.05.002
638   Dougall, D.K., Baker, D.C., 2008. Effects of reaction mixture and other components on the
639   determination of the equilibrium and rate constants of the hydration reactions of
640   anthocyanins. Food Chem. 107, 473–482. doi:10.1016/j.foodchem.2007.07.035
641   Féret, J.-B., François, C., Asner, G.P., Gitelson, A.A., Martin, R.E., Bidel, L.P.R., Ustin, S.L., le Maire, G.,
642   Jacquemoud, S., 2008. PROSPECT-4 and 5: Advances in the leaf optical properties model
643   separating photosynthetic pigments. Remote Sens. Environ. 112, 3030–3043.
644   doi:10.1016/j.rse.2008.02.012
645   Féret, J.-B., François, C., Gitelson, A., Asner, G.P., Barry, K.M., Panigada, C., Richardson, A.D.,
646   Jacquemoud, S., 2011. Optimizing spectral indices and chemometric analysis of leaf chemical
647   properties using radiative transfer modeling. Remote Sens. Environ. 115, 2742–2750.
648   doi:10.1016/j.rse.2011.06.016
649   Figueiredo, P., George, F., Tatsuzawa, F., Toki, K., Saito, N., Brouillard, R., 1999. New features of
650   intramolecular copigmentation byacylated anthocyanins. Phytochemistry 51, 125–132.
651   doi:10.1016/S0031-9422(98)00685-2
652   Filella, I., Porcar-Castell, A., Munné-Bosch, S., Bäck, J., Garbulsky, M.F., Peñuelas, J., 2009. PRI
653   assessment of long-term changes in carotenoids/chlorophyll ratio and short-term changes in
654   de-epoxidation state of the xanthophyll cycle. Int. J. Remote Sens. 30, 4443–4455.
655   doi:10.1080/01431160802575661
656   Fossen, T., Cabrita, L., Andersen, O.M., 1998. Colour and stability of pure anthocyanins influenced by
657   pH including the alkaline region. Food Chem. 63, 435–440. doi:10.1016/S0308-
658   8146(98)00065-X
659   Fukshansky, L., Remisowsky, A.M.V., McClendon, J., Ritterbusch, A., Richter, T., Mohr, H., 1993.
660   Absorption spectra of leaves corrected for scattering and distributional error: a radiative
661   transfer and absorption statistics treatment. Photochem. Photobiol. 57, 538–555.
662   doi:10.1111/j.1751-1097.1993.tb02332.x
663   Gamon, J.A., Field, C.B., Bilger, W., Björkman, O., Fredeen, A.L., Peñuelas, J., 1990. Remote sensing of
664   the xanthophyll cycle and chlorophyll fluorescence in sunflower leaves and canopies.
665   Oecologia 85, 1–7. doi:10.1007/BF00317336

666 Gamon, J.A., Huemmrich, K.F., Wong, C.Y.S., Ensminger, I., Garrity, S., Hollinger, D.Y., Noormets, A.,
667   Peñuelas, J., 2016. A remotely sensed pigment index reveals photosynthetic phenology in
668   evergreen conifers. Proc. Natl. Acad. Sci. 113, 13087–13092. doi:10.1073/pnas.1606162113
669 Gamon, J.A., Peñuelas, J., Field, C.B., 1992. A narrow-waveband spectral index that tracks diurnal
670   changes in photosynthetic efficiency. Remote Sens. Environ. 41, 35–44. doi:10.1016/0034-
671   4257(92)90059-S
672 Gamon, J.A., Serrano, L., Surfus, J.S., 1997. The photochemical reflectance index: an optical indicator
673   of photosynthetic radiation use efficiency across species, functional types, and nutrient
674   levels. Oecologia 112, 492–501. doi:10.1007/s004420050337
675 Gamon, J.A., Surfus, J.S., 1999. Assessing leaf pigment content a nd activity with a reflectometer.
676   New Phytol. 105–117.
677 Gastellu-Etchegorry, J.-P., Yin, T., Lauret, N., Cajgfinger, T., Gregoire, T., Grau, E., Féret, J.-B., Lopes,
678   M., Guilleux, J., Dedieu, G., Malenovský, Z., Cook, B., Morton, D., Rubio, J., Durrieu, S.,
679   Cazanave, G., Martin, E., Ristorcelli, T., 2015. Discrete anisotropic radiative transfer (DART 5)
680   for modeling airborne and satellite spectroradiometer and LIDAR acquisitions of natural and
681   urban landscapes. Remote Sens. 7, 1667–1701. doi:10.3390/rs70201667
682 Gitelson, A.A., 2005. Remote estimation of canopy chlorophyll content in crops. Geophys. Res. Lett.
683   32. doi:10.1029/2005GL022688
684 Gitelson, A.A., Chivkunova, O.B., Merzlyak, M.N., 2009. Nondestructive estimation of anthocyanins
685   and chlorophylls in anthocyanic leaves. Am. J. Bot. 96, 1861–1868. doi:10.3732/ajb.0800395
686 Gitelson, A.A., Keydan, G.P., Merzlyak, M.N., 2006. Three-band model for noninvasive estimation of
687   chlorophyll, carotenoids, and anthocyanin contents in higher plant leaves. Geophys. Res.
688   Lett. 33, L11402. doi:10.1029/2006GL026457
689 Gitelson, A.A., Merzlyak, M.N., Chivkunova, O.B., 2001. Optical properties and nondestructive
690   estimation of anthocyanin content in plant leaves. Photochem. Photobiol. 74, 38–45.
691   doi:10.1562/0031-8655(2001)074<0038:OPANEO>2.0.CO;2
692 Gitelson, A.A., Peng, Y., Masek, J.G., Rundquist, D.C., Verma, S., Suyker, A., Baker, J.M., Hatfield, J.L.,
693   Meyers, T., 2012. Remote estimation of crop gross primary production with Landsat data.
694   Remote Sens. Environ. 121, 404–414. doi:10.1016/j.rse.2012.02.017
695 Gould, K., Davies, K., Winefield, C. (Eds.), 2009. Anthocyanins: Biosynthesis, functions, and
696   applications. Springer, New York, NY.
697 Gould, K.S., 2004. Nature's swiss army knife: The diverse protective roles of anthocyanins in leaves. J.
698   Biomed. Biotechnol. 2004, 314–320. doi:10.1155/S1110724304406147
699 Haboudane, D., 2004. Hyperspectral vegetation indices and novel algorithms for predicting green LAI
700   of crop canopies: Modeling and validation in the context of precision agriculture. Remote
701   Sens. Environ. 90, 337–352. doi:10.1016/j.rse.2003.12.013
702 Hale, G.M., Querry, M.R., 1973. Optical constants of water in the 200-nm to 200-μm wavelength
703   region. Appl. Opt. 12, 555–562. doi:10.1364/AO.12.000555
704 Harborne, J.B., Williams, C.A., 1998. Anthocyanins and other flavonoids. Nat. Prod. Rep. 15, 631–652.
705   doi:10.1039/a815631y
706 Hernández-Clemente, R., Navarro-Cerrillo, R.M., Zarco-Tejada, P.J., 2014. Deriving predictive
707   relationships of carotenoid content at the canopy level in a conifer forest using hyperspectral
708   imagery and model simulation. IEEE Trans. Geosci. Remote Sens. 52, 5206–5217.
709   doi:10.1109/TGRS.2013.2287304
710 Hernández-Clemente, R., Navarro-Cerrillo, R.M., Zarco-Tejada, P.J., 2012. Carotenoid content
711   estimation in a heterogeneous conifer forest using narrow-band indices and PROSPECT+
712   DART simulations. Remote Sens. Environ. 127, 298–315. doi:doi:10.1016/j.rse.2012.09.014
713 Hmimina, G., Merlier, E., Dufrêne, E., Soudani, K., 2015. Deconvolution of pigment and
714   physiologically related photochemical reflectance index variability at the canopy scale over
715   an entire growing season: Towards an understanding of canopy PRI variability. Plant Cell
716   Environ. 38, 1578–1590. doi:10.1111/pce.12509

717 Jacquemoud, S., Baret, F., 1990. PROSPECT: A model of leaf optical properties spectra. Remote Sens.
718   Environ. 34, 75–91. doi:10.1016/0034-4257(90)90100-Z
719 Jacquemoud, S., Verhoef, W., Baret, F., Bacour, C., Zarco-Tejada, P.J., Asner, G.P., François, C., Ustin,
720   S.L., 2009. PROSPECT+ SAIL models: A review of use for vegetation characterization. Remote
721   Sens. Environ. 113, S56–S66. doi:doi:10.1016/j.rse.2008.01.026
722 Jay, S., Bendoula, R., Hadoux, X., Féret, J.-B., Gorretta, N., 2016. A physically-based model for
723   retrieving foliar biochemistry and leaf orientation using close-range imaging spectroscopy.
724   Remote Sens. Environ. 177, 220–236. doi:10.1016/j.rse.2016.02.029
725 Joiner, J., Yoshida, Y., Vasilkov, A.P., Yoshida, Y., Corp, L.A., Middleton, E.M., 2011. First observations
726   of global and seasonal terrestrial chlorophyll fluorescence from space. Biogeosciences 8,
727   637–651. doi:10.5194/bg-8-637-2011
728 le Maire, G., François, C., Dufrêne, E., 2004. Towards universal broad leaf chlorophyll indices using
729   PROSPECT simulated database and hyperspectral reflectance measurements. Remote Sens.
730   Environ. 89, 1–28. doi:10.1016/j.rse.2003.09.004
731 Lee, D., Gould, K., 2002. Why Leaves Turn Red: : Pigments called anthocyanins probably protect
732   leaves from light damage by direct shielding and by scavenging free radicals,. Am. Sci. 90,
733   524–528. doi:10.1511/2002.6.524
734 Lev-Yadun, S., Gould, K.S., 2008. Role of anthocyanins in plant defence, in: Winefield, C., Davies, K.,
735   Gould, K. (Eds.), Anthocyanins. Springer New York, New York, NY, pp. 22–28.
736 Li, P., Wang, Q., 2011. Retrieval of leaf biochemical parameters using PROSPECT inversion: A new
737   approach for alleviating ill-posed problems. IEEE Trans. Geosci. Remote Sens. 49, 2499–2506.
738   doi:10.1109/TGRS.2011.2109390
739 Lucarini, V., Saarinen, J.J., Peiponen, K.-E., Vartiainen, E.M. (Eds.), 2005. Kramers-Kronig relations in
740   optical materials research, Springer series in optical sciences. Springer, Berlin.
741 Maier, S.W., Lüdeker, W., Günther, K.P., 1999. SLOP: : a revised version of the stochastic model for
742   leaf optical properties. Remote Sens. Environ. 68, 273–280. doi:10.1016/S0034-
743   4257(98)00118-7
744 Malenovský, Z., Albrechtová, J., Lhotáková, Z., Zurita-Milla, R., Clevers, J.G.P.W., Schaepman, M.E.,
745   Cudlín, P., 2006. Applicability of the PROSPECT model for Norway spruce needles. Int. J.
746   Remote Sens. 27, 5315–5340. doi:10.1080/01431160600762990
747 Marquart, L.C., 1835. Die Farben der Blüthen: Eine Chemisch-Physiologische Abhandlung. Verlag von
748   T. Habicht, Bonn.
749 Martinière, A., Bassil, E., Jublanc, E., Alcon, C., Reguera, M., Sentenac, H., Blumwald, E., Paris, N.,
750   2013. In vivo intracellular pH measurements in tobacco and arabidopsis reveal an
751   unexpected pH gradient in the endomembrane system. Plant Cell 25, 4028–4043.
752   doi:10.1105/tpc.113.116897
753 Mathieu, Y., Guern, J., Kurkdjian, A., Manigault, P., Manigault, J., Zielinska, T., Gillet, B., Beloeil, J.-C.,
754   Lallemand, J.-Y., 1989. Regulation of vacuolar pH of plant cells: I. isolation and properties of
755   vacuoles suitable for ^{31}P NMR studies. Plant Physiol. 89, 19–26. doi:10.1104/pp.89.1.19
756 Matile, P., 2000. Biochemistry of Indian summer: physiology of autumnal leaf coloration. Exp.
757   Gerontol. 35, 145–158. doi:10.1016/S0531-5565(00)00081-4
758 Merzlyak, M.N., Chivkunova, O.B., Solovchenko, A.E., Naqvi, K.R., 2008. Light absorption by
759   anthocyanins in juvenile, stressed, and senescing leaves. J. Exp. Bot. 59, 3903–3911.
760   doi:10.1093/jxb/ern230
761 Nakaji, T., Oguma, H., Fujinuma, Y., 2006. Seasonal changes in the relationship between
762   photochemical reflectance index and photosynthetic light use efficiency of Japanese larch
763   needles. Int. J. Remote Sens. 27, 493–509. doi:10.1080/01431160500329528
764 Peng, Y., Gitelson, A.A., 2012. Remote estimation of gross primary productivity in soybean and maize
765   based on total crop chlorophyll content. Remote Sens. Environ. 117, 440–448.
766   doi:10.1016/j.rse.2011.10.021
767 Peters, R.D., Noble, S.D., 2014. Spectrographic measurement of plant pigments from 300 to 800nm.
768   Remote Sens. Environ. 148, 119–123. doi:10.1016/j.rse.2014.03.020

769 Pfündel, E.E., Ben Ghozlen, N., Meyer, S., Cerovic, Z.G., 2007. Investigating UV screening in leaves by
770   two different types of portable UV fluorimeters reveals in vivo screening by anthocyanins
771   and carotenoids. Photosynth. Res. 93, 205–221. doi:10.1007/s11120-007-9135-7
772 Richardson, A.D., Duigan, S.P., Berlyn, G.P., 2002. An evaluation of noninvasive methods to estimate
773   foliar chlorophyll content. New Phytol. 153, 185–194. doi:10.1046/j.0028-646X.2001.00289.x
774 Rühle, W., Wild, A., 1979. The intensification of absorbance changes in leaves by light-dispersion:
775   Differences between high-light and low-light leaves. Planta 146, 551–557.
776   doi:10.1007/BF00388831
777 Rundquist, D., Gitelson, A., Leavitt, B., Zygielbaum, A., Perk, R., Keydan, G., 2014. Elements of an
778   integrated phenotyping system for monitoring crop status at canopy level. Agronomy 4, 108–
779   123. doi:10.3390/agronomy4010108
780 Shipley, B., Lechowicz, M.J., Wright, I., Reich, P.B., 2006. Fundamental trade-offs generating the
781   worldwide leaf economics spectrum. Ecology 87, 535–541. doi:10.1890/05-1051
782 Sims, D.A., Gamon, J.A., 2002. Relationships between leaf pigment content and spectral reflectance
783   across a wide range of species, leaf structures and developmental stages. Remote Sens.
784   Environ. 81, 337–354. doi:10.1016/S0034-4257(02)00010-X
785 Solovchenko, A.E., Chivkunova, O.B., Merzlyak, M.N., Reshetnikova, I.V., 2001. A spectrophotometric
786   analysis of pigments in apples. Russ. J. Plant Physiol. 48, 693–700.
787   doi:10.1023/A:1016780624280
788 Steele, M.R., Gitelson, A.A., Rundquist, D.C., Merzlyak, M.N., 2009. Nondestructive estimation of
789   anthocyanin content in grapevine leaves. Am. J. Enol. Vitic. 60, 87–92.
790 Stuckens, J., Verstraeten, W.W., Delalieux, S., Swennen, R., Coppin, P., 2009. A dorsiventral leaf
791   radiative transfer model: Development, validation and improved model inversion techniques.
792   Remote Sens. Environ. 113, 2560–2573. doi:10.1016/j.rse.2009.07.014
793 Stylinski, C., Gamon, J., Oechel, W., 2002. Seasonal patterns of reflectance indices, carotenoid
794   pigments and photosynthesis of evergreen chaparral species. Oecologia 131, 366–374.
795   doi:10.1007/s00442-002-0905-9
796 Ustin, S.L., Gitelson, A.A., Jacquemoud, S., Schaepman, M., Asner, G.P., Gamon, J.A., Zarco-Tejada, P.,
797   2009. Retrieval of foliar information about plant pigment systems from high resolution
798   spectroscopy. Remote Sens. Environ. 113, S67–S77. doi:10.1016/j.rse.2008.10.019
799 van den Berg, A.K., Perkins, T.D., 2005. Nondestructive estimation of anthocyanin content in autumn
800   sugar maple leaves. HortScience 40, 685–686.
801 Verhoef, W., 1984. Light scattering by leaf layers with application to canopy reflectance modeling:
802   The SAIL model. Remote Sens. Environ. 16, 125–141. doi:10.1016/0034-4257(84)90057-9
803 Verhoef, W., Jia, L., Xiao, Q., Su, Z., 2007. Unified optical-thermal four-stream radiative transfer
804   theory for homogeneous vegetation canopies. IEEE Trans. Geosci. Remote Sens. 45, 1808–
805   1822. doi:10.1109/TGRS.2007.895844
806 Verrelst, J., Camps-Valls, G., Muñoz-Marí, J., Rivera, J.P., Veroustraete, F., Clevers, J.G.P.W., Moreno,
807   J., 2015. Optical remote sensing and the retrieval of terrestrial vegetation bio-geophysical
808   properties – A review. ISPRS J. Photogramm. Remote Sens. 108, 273–290.
809   doi:10.1016/j.isprsjprs.2015.05.005
810 Yabuya, T., Nakamura, M., Iwashina, T., Yamaguchi, M., Takehara, T., 1997. Anthocyanin-flavone
811   copigmentation in bluish purple flowers of Japanese garden iris (*Iris ensata* Thunb.).
812   Euphytica 98, 163–167. doi:10.1023/A:1003152813333
813 Zarco-Tejada, P.J., Guillén-Climent, M.L., Hernández-Clemente, R., Catalina, A., González, M.R.,
814   Martín, P., 2013. Estimating leaf carotenoid content in vineyards using high resolution
815   hyperspectral imagery acquired from an unmanned aerial vehicle (UAV). Agric. For.
816   Meteorol. 171–172, 281–294. doi:10.1016/j.agrformet.2012.12.013
817

818   **Figure 1.** Relationship between C_{anth} obtained from wet chemistry and C_{anth} estimated from

819   reflectance data after application of Eq. 2. The black dots correspond to the 137 leaf samples with

820   $mARI < 5$ (R^2 = 0.90) and the grey dots correspond to the 76 leaf samples with $mARI > 5$ (R^2 =

821   0.37). Eq. 2 was adjusted only on the black dots.

822

823   **Figure 2.** Comparison of the refractive index used in PROSPECT-3 (red dots), PROSPECT-5 (grey

824   diamonds) and corresponding to the mean refractive index proposed by (Chen and Weng, 2012)

825   (blue squares). The grey area corresponds to the range of variation of the refractive index proposed

826   by Chen and Weng, (2012); the plain grey line corresponds to the refractive index for pure liquid

827   water (Hale and Querry, 1973).

828

829   **Figure 3.** Stacked distribution of pigment content for the calibration and validation samples selected

830   from ANGERS and VIRGINIA. Light colors: calibration (144 samples from ANGERS, 20 Samples from

831   VIRGINIA); dark colors: validation (164 samples from ANGERS, 61 samples from VIRGINIA).

832

833   **Figure 4.** Spectral RMSE between measured leaf optics and simulated reflectance (left), and

834   transmittance (right) obtained after model inversion with the refractive index used in PROSPECT-5

835   (black dotted line), PROSPECT-3 (red), and derived from Chen and Weng (2012) (light grey).

836

837   **Figure 5.** Specific absorption coefficients of chlorophylls (green), carotenoids (orange), and

838   anthocyanins (red). The solids line correspond to the SAC of all the pigments in PROSPECT-D, the

839   dashed lines to the SAC of chlorophylls and carotenoids in PROSPECT-5, and to the SAC of

840   anthocyanins measured by Peters and Noble (2014) using thin layer chromatography.

841

842 **Figure 6.** Estimation of pigment content by inversion of three versions of PROSPECT on six datasets

843 (when relevant). Red dots correspond to calibration samples from ANGERS and VIRGINIA.

844

845 **Figure 7.** Spectral RMSE between measured and estimated leaf reflectance and transmittance

846 obtained for the VALIDATION dataset after model inversion using PROSPECT-3, PROSPECT-5, and

847 PROSPECT-D.

848

849 **Figure 8.** Comparison of the SACs obtained for the three pigments when using C_{anth} values directly

850 derived from $mARI$ (dashed lines) and when using C_{anth} values with noise added corresponding to

851 the error of prediction of C_{anth} observed for experimental data (50 repetitions; plain lines and their

852 envelope correspond to mean value ± 1 standard deviation).

853

854 **Figure 9.** Distribution of the RMSE between measured and estimated pigment content after adding

855 noise to the values of C_{anth} of ANGERS used for calibration of PROSPECT and inversion of the model

856 based on the SACs displayed in Figure 8. Colored dots correspond to the RMSE obtained when no

857 noise is added to C_{anth} in ANGERS.

858

859 **Figure 10.** Spectral RMSE between measured and estimated leaf reflectance and transmittance

860 obtained for the VALIDATION dataset after model inversion using PROSPECT-D calibrated with (grey

861 lines) and without (red lines) uncertainty added to C_{anth}.

862

863 **Figure 11.** Comparison of the SAC corresponding to anthocyanins derived from PROSPECT-D

864 calibration ($cm^2\ \mu g^{-1}$) and the absorption of pure Cyanidin 3-glucoside at pH 1 and 8.1 (unitless) (after

865 Fossen et al., 1998).

866

867   **Figure 12.** Measured (black dotted line) versus simulated (blue line for PROSPECT-5 and red line for

868   PROSPECT-D) reflectance (lower spectra) and transmittance (upper spectra). (a-b) *Acer*

869   *pseudoplatanus* L., (c) *Acer platanoides* L., (d) *Corylus avellana* L., (e-f) *Parthenocissus quinquefolia*

870   (L.) Planch., (g) *Corylus maxima 'Purpurea'*, and (h) *Eucalyptus gunnii*. Samples (b-e-f) show non-

871   senescent anthocyanic leaves, while samples (a-c-d-g) show anthocyanic senescent leaves.

872

873   **Table 1.** Description of the leaf datasets used in this study.

874

875   **Table 2.** RMSE ($\mu g\ cm^{-2}$) of the estimation of leaf pigment content using PROSPECT-3 (P-3),

876   PROSPECT-5 (P-5), and PROSPECT-D (P-D) inversion. The bold font for numbers indicates the lowest

877   values.

878